Received 31 March 2021; revised 5 May 2021; accepted 17 May 2021. Date of publication 21 May 2021; date of current version 2 June 2021.

*Digital Object Identifier 10.1109/OJCOMS.2021.3082688*

# Enhanced Uplink Coverage for 5G NR: Frequency-Domain Spectral Shaping With Spectral Extension

**ISMAEL PERUGA NASARRE[1], TONI LEVANEN[1,2], KARI PAJUKOSKI[3], ARTO LEHTI[4], ESA TIIROLA[3], AND MIKKO VALKAMA[1] (Senior Member, IEEE)**

[1]Department of Electrical Engineering, Tampere University, 33720 Tampere, Finland

[2]Nokia Mobile Networks, 33100 Tampere, Finland

[3]Nokia Bell Labs, 90620 Oulu, Finland

[4]Nokia Bell Labs, 91620 Paris-Saclay, France

CORRESPONDING AUTHOR: M. VALKAMA (e-mail: mikko.valkama@tuni.fi)

This work was supported in part by the Academy of Finland under Grant 319994 and Grant 332361; in part by Finnish Funding Agency for Innovation under Project 5G-FORCE; and in part by Nokia Bell Labs.

**ABSTRACT** This paper describes and investigates a novel concept of frequency-domain spectral shaping (FDSS) with spectral extension for the uplink (UL) coverage enhancement in 5G New Radio (NR), building on discrete Fourier transform spread orthogonal frequency-domain multiplexing (DFT-s-OFDM). The considered FDSS concept is shown to have large potential for reducing the peak-to-average-power ratio (PAPR) of the signal, which directly impacts the feasible maximum transmit power under practical nonlinear power amplifiers (PAs) while still meeting the radio frequency (RF) emission requirements imposed by the regulations. To this end, the FDSS scheme with spectral extension is formulated, defining filter windows that fit to the 5G NR spectral flatness requirements. The PAPR reduction capabilities and the corresponding maximum achievable transmit powers are evaluated for a variety of bandwidth allocations in the supported 5G NR frequency ranges 1 and 2 (FR1 and FR2) and compared to those of the currently supported waveforms in 5G NR, particularly $\pi/2$-BPSK with FDSS without spectral extension and QPSK without FDSS. Furthermore, an efficient receiver structure capable of reducing the noise enhancement in the equalization phase is proposed. Finally, by evaluating the link-level performance, together with the transmit power gain, the overall coverage enhancement gains of the method are analyzed and provided. The obtained results show that the spectrally-extended FDSS method is a very efficient solution to improve the 5G NR UL coverage clearly outperforming the state-of-the-art, while being also simple in terms of computational complexity such that the method is implementation feasible in practical 5G NR terminals.

**INDEX TERMS** 5G new radio evolution, coverage, DFT-s-OFDM, energy-efficiency, frequency-domain spectral shaping, peak-to-average-power ratio, radio link performance, transmitter requirements.

## I. INTRODUCTION

NETWORK coverage is of fundamental importance in all wireless communications systems. One of the current trends is to utilize substantially higher frequency bands, particularly the so-called millimeter-wave (mmWave) frequencies of 30–300 GHz for mobile access [1], offering large chunks of available spectrum for increased throughputs and reduced latencies. However, the corresponding propagation conditions become more challenging [2] while the quality and efficiency of the radio frequency (RF) electronics are also simultaneously reducing [3]. These imply clear needs for finding efficient coverage enhancement methods in the evolving mmWave networks. Additionally, coverage enhancement needs are not only limited to higher frequency

bands, but also the networks within 0–6 GHz bands can benefit from improved coverage, e.g., in case of mobile broadband service in rural areas or when connecting Internet-of-Things (IoT) sensors in deep-indoor environments to the macro networks [4]. In this article, the main emphasis is on describing and studying uplink (UL) coverage enhancement techniques that are computationally feasible for mobile terminals and that can be supported in the 3rd Generation Partnership Project (3GPP) 5G New Radio (NR) standardization through straight-forward refinements without requiring any larger redesign of the system and the radio interface.

### A. STATE-OF-THE-ART

The 3GPP has been systematically working towards facilitating better network coverage and longer battery lifetime for user equipment (UE) through enhancements in the cellular mobile radio standards. This covers, e.g., a new UE Category 0 with reduced RF and baseband complexity, introduced already in Long Term Evolution (LTE) release (Rel) 12 [5] for the purpose of reducing the power consumption of IoT devices. Additionally, two new categories with narrowband transmission focus, the Category M1 and Category NB1, were introduced in LTE Rel-13 [5] with specific emphasis on IoT and machine type communications (MTC). These categories are specifically targeting to facilitate reliable communication over existing networks while also providing longer operational times for battery-powered mobile or stationary devices compared to other LTE devices.

More recently, 3GPP started a study item [6] to identify the coverage bottlenecks at frequency range 1 (FR1, 410 MHz – 7125 MHz) and frequency range 2 (FR2, the mmWave bands 24250 MHz – 52600 MHz), defined in [7], by means of link budget analysis based on the IMT-2020 self-evaluation template [8], while also investigating different solutions for solving the identified challenges. The objective of the study item is to capture the results in a technical report (TR) for 5G NR Rel-17 [9]. Stemming from this, different bodies have identified the coverage bottlenecks that exist in 5G NR Rel-16 by performing extensive radio link simulations for specific deployment and service scenarios such as urban, indoor, enhanced mobile broadband (eMBB), etc, while using the link budget template to identify the problematic physical channels. To this end, a vast majority of the contributions concluded that the physical uplink shared channel (PUSCH) is one clear coverage bottleneck at both FR1 and FR2, especially for eMBB service. Furthermore, with emphasis on MTC, 3GPP started a study on reduced capability NR devices [10].

In general, different solutions can be devised and applied to obtain improved coverage. In [5], a survey on different techniques with MTC emphasis is provided, including methods such as relaxed RF requirements, narrowband operation, time repetition, or frequency diversity. In [11], improved coding gain by means of utilizing *a priori* known bits in the receiver is shown to improve the effective signal-to-noise ratio (SNR) of the physical broadcast channel (PBCH) and thus the corresponding detection performance. In time-domain, coverage enhancement may be acquired by repetitions [12], however, when applying time repetition, the power consumption of the device typically increases. Also frequency-domain based solutions may be used, such as inter or intra-slot frequency hopping [13]. It is noted that the frequency-domain spectral shaping (FDSS) solution described in this paper is also shown to offer in-built frequency diversity when spectral extension is properly used in the receiver. Finally, spatial-domain solutions in terms of multi-antenna transmission and processing may achieve improved coverage, however, in small form-factor devices like phones or dedicated MTC sensors, the amount of antennas and corresponding power amplifiers (PAs) can easily be limited. In larger devices, e.g., cars or industrial vehicles, this is more viable.

In the power domain, by using waveforms with low peak-to-average-power ratio (PAPR), larger output power can in general be obtained from a given PA system under given emission constraints and transmit signal passband quality requirements. This directly increases the SNR in the receiver, or alternatively allows for larger link distances. In [14], a new coded or constrained modulation scheme was proposed which reduces the phase variations between consecutive transmitted symbols. This results in a signal with low PAPR, that can also be tuned based on different parameters. In [15], the authors proposed a novel technique based on the superposition of several pulse-shaped discrete Fourier transform spread orthogonal frequency-domain multiplexing (DFT-s-OFDM) signals, where the obtained signal presents low PAPR characteristics. The proposal in [16], in turn, follows a similar approach, where a low PAPR filter bank for single-carrier frequency division multiple access (SC-FDMA) is used, allowing to reduce the out-of-band (OOB) emissions at the PA output. In such approach, multiple streams can be used to further reduce the PAPR.

Furthermore, well-known processing methods to provide enhancements in the power domain are the iterative clipping and filtering (ICF) [17] as well as tone reservation [18] techniques. These methods have been traditionally used for multicarrier transmissions, but can basically be also applied in the single-carrier context. However, these methods present a substantial processing complexity that includes several iterations where DFT/inverse DFT (IDFT) pairs need to be performed. Thus, this has commonly challenged their applicability at UE/terminal side, particularly at FR2 where the processing bandwidths are very large.

Finally, it is noted that alternative modulation or physical-layer approaches, such as offset quadrature phase shift keying (OQPSK) [19], offset quadrature amplitude modulation (OQAM) applied through filter bank multicarrier (FBMC) processing [20], generalized frequency division multiplexing (GFDM) [21], block-windowed burst (BWB) OFDM [22], and time-interleaved BWB-OFDM [23] have

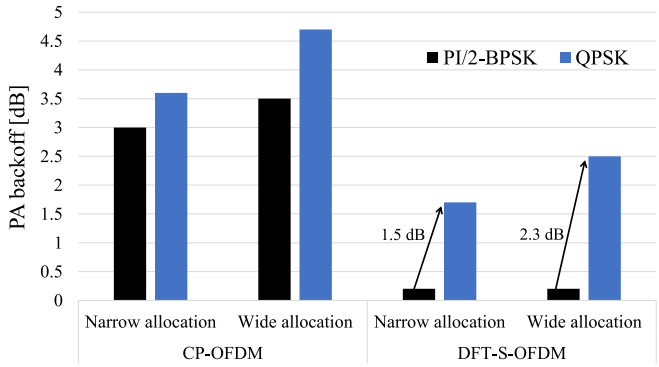


**FIGURE 1.** Comparative illustration of the PA backoff values required by different modulations when noting the 3GPP FR2 requirements for OOB emissions and passband waveform quality. For $\pi/2$-BPSK, FDSS is already considered according to Rel-15 specifications while basic BPSK is assumed in CP-OFDM case. Narrow and wide allocations correspond to 8 PRBs and 256 PRBs, respectively, while 400 MHz channel bandwidth and subcarrier spacing of 120 kHz are assumed.

been proposed in the literature, with different tradeoffs between spectrum localization, resource allocation flexibility, multiantenna support, power-efficiency and transceiver processing complexity. These methods would, however, in most cases call for larger redesign of the 5G NR physical-layer specifications, and are thus not explicitly considered in the rest of this article.

### B. CONTRIBUTIONS AND ORGANIZATION

In this paper, we describe and study an efficient yet computationally simple FDSS method with spectral extension on top of the baseline DFT-s-OFDM or SC-FDMA processing. This solution allows to reduce the PAPR and therefore to increase the UE transmit power – or in 3GPP terminology, relax the so-called maximum power reduction (MPR) constraints. The considered approach is computationally very simple in the sense that only two new blocks are added on top of the traditional DFT-s-OFDM transmitter, namely the symmetric extension block and the frequency-domain point-to-point product between the subcarrier samples and the filtering weights. While one form of spectral shaping is already defined in 5G NR Rel-15 for $\pi/2-$BPSK, in this work we extend and generalize the concept for higher-order modulations, particularly QPSK. There is a substantial motivation for this since as illustrated in Fig. 1, there exists a very big gap in the needed baseline PA backoff values when increasing the modulation order from BPSK to QPSK. Thus, the proposed solution can potentially reduce the backoff and largely improve the coverage accordingly [13], while still meeting the OOB emission and passband signal quality requirements. Additionally, the impacts of the proposed method on the receiver side are addressed. Specifically, we describe how the transmit signal spectral extension can be utilized in the receiver signal processing to provide frequency diversity, hence improving the detection performance. Furthermore, we address in detail the spectral shaping filter or mask design at transmitter side, through truncated root raised-cosine (RRC) windows, while taking into account the 3GPP requirements for spectral flatness. Also, a very extensive set of numerical results is provided, in terms of achievable PAPR reduction, transmit power gains, radio link performance and the corresponding overall coverage gains. Finally, the effects of FDSS on UL demodulation reference signals are shortly addressed.

The remainder of the paper is structured as follows. Section II first reviews the mathematical basics of the DFT-s-OFDM transmitter and the corresponding time-domain pulses. Then, the proposed FDSS method with spectral extension is described, followed by the receiver signal processing developments and the transmitter filtering window or mask design procedures. Then, in Section III, we describe the performance evaluation methodology and metrics, while Section IV presents and analyzes the large collection of numerical results. Finally, the conclusions are drawn in Section V.

## II. SYSTEM MODEL AND PROPOSED METHODS

### A. DFT-S-OFDM AND TIME-DOMAIN PULSES

DFT-s-OFDM is a well-known modulation and multiple access scheme that has gained popularity in wireless communications, especially in scenarios where transmitter power-efficiency is important. Good example is uplink (UL) of LTE-technology based networks [24] while it is also supported in the UL of 5G NR [25] in parallel with cyclic prefix (CP)-OFDM. A comprehensive analysis of DFT-s-OFDM can be found, e.g., in [26], while below we also shortly review the fundamentals.

The processing chain for DFT-s-OFDM contains first a DFT of the $M$ input complex sub-symbols,[1] denoted by $s(m)$ with $m \in \{0, \ldots, M-1\}$, that are transmitted within one DFT-s-OFDM symbol. The corresponding frequency-domain samples at the DFT output can be formally expressed as

$$X(k) = \frac{1}{\sqrt{M}} \sum_{m=0}^{M-1} s(m) e^{-j\frac{2\pi km}{M}}, \tag{1}$$

for $k \in \mathcal{K}_d$, where $\mathcal{K}_d$ is the set of active data subcarriers. In a traditional DFT-s-OFDM modulator, after the DFT, the $M$ point frequency-domain sequence $X(k)$ is zero-padded and converted to time-domain through IDFT of size $N > M$. The corresponding discrete-time sequence reads

$$x(n) = \frac{1}{\sqrt{N}} \sum_{k \in \mathcal{K}_d} X(k) e^{j\frac{2\pi kn}{N}}, \tag{2}$$

where $n \in \{0, 1, \ldots, N-1\}$ is the time-domain sample index within one DFT-s-OFDM symbol. The single-carrier flavor of DFT-s-OFDM can be established via combining (1)

1. Sub-symbols are referring to the group of complex modulated symbols that are part of one DFT-s-OFDM symbol.

and (2) [27], yielding

$$x(n) = \frac{1}{\sqrt{M}} \sum_{m=0}^{M-1} s(m) \underbrace{\frac{1}{\sqrt{N}} \sum_{k \in \mathcal{K}_d} e^{j\frac{2\pi k}{N}\left(n - \frac{mN}{M}\right)}}_{g\left(n - \frac{mN}{M}\right)}. \tag{3}$$

where $g(v)$ is the effective pulse-shape function. Assuming that the active data subcarriers are allocated at the center of the channel, expressed as $\mathcal{K}_d = \{-M/2, -M/2 + 1, \ldots, M/2 - 1\}$, $g(v)$ can be shown to read

$$g(v) = \frac{1}{\sqrt{N}} e^{-j\frac{\pi v}{N}} \frac{\sin\left(\frac{\pi M v}{N}\right)}{\sin\left(\frac{\pi v}{N}\right)}. \tag{4}$$

For other sets of contiguous allocations, the expression in (4) is similar except for the phase term.

Based on (3), the pulse-shape $g(v)$ is effectively modulated by the complex sub-symbols with the corresponding time shifts ($\frac{mN}{M}$ for the $m$th sub-symbol $s(m)$) and all the $M$ pulses are combined to obtain the baseband waveform. The pulse-shape $g(v)$ corresponds to a cyclically-periodic sinc-like function with period $N$ and first null at $N/M$, or alternatively to a frequency-domain square pulse of $M$ samples.

A basic illustration of the periodic sinc-like pulses is given in Fig. 2(a). Like can be observed, the pulse-sidelobes are heavily overlapping and thus when combining coherently, can create large peaks in the time-domain waveform. Thus, further shaping of the pulses is beneficial in order to reduce the PAPR of the signal. Inspired by this, the proposed FDSS concept seeks to create pulses that decay faster than the basic periodic sinc-like pulses, thus reducing the PAPR. Furthermore, the spectral extension provides a larger time separation of the neighboring pulses, improving the PAPR even further. These are described and discussed in detail next.

### B. FREQUENCY-DOMAIN SPECTRAL SHAPING WITH SPECTRAL EXTENSION

Let us first define some of the main quantities for presentation clarity. The so-called total allocation size, $Q$, is the number of frequency-domain resources (also referred to as subcarriers, frequency bins, or in 3GPP notation, resource elements, RE) that are used for transmission. These $Q$ resources carry the in-band – and if so noted – also the excess band transmit signal contents. As in-band, we refer to the $M \leq Q$ frequency-domain resources that carry the data, and it is further assumed that the in-band is located in the middle of the allocation for conceptual simplicity. The excess band, in turn, corresponds to the $E$ frequency-domain resources that are obtained after symmetric extension of the in-band, and it is further assumed that $E/2$ frequency-domain resources are allocated at one side of the in-band, and the other $E/2$ resources are allocated in the other side. With a fixed total allocation size $Q$, the extension in percentage is defined as $(1 - M/Q) \times 100$. Finally, for notational simplicity, we index the total allocation bins in the rest of the paper as $k = 0, \ldots, Q - 1$, while note that the exact true IFFT bins depend on the location of the total allocation within the channel bandwidth.

Building on above definitions, Fig. 3 illustrates the block-diagram of a DFT-s-OFDM transmitter incorporating the proposed FDSS with symmetric spectral extension (highlighted in gray background). The symmetric spectral extension is performed between the DFT and the IFFT stages, yielding $Q$ subcarriers, where $Q = M + E$ is the size of the total resource allocation and $E$ is the total excess band in subcarriers as discussed above. To this end, the symmetrical spectrally extended version of the DFT output can be expressed as

$$X'(k) = X\left(\left(k + M - \frac{E}{2}\right), \text{mod } M\right), \tag{5}$$

for $k = 0, \ldots, Q - 1$ where mod $M$ represents the modulo operation with respect to $M$. The symmetric spectral extension, with roots already in [28], is performed by copying $\frac{E}{2}$ subcarriers from one side of the DFT output and placing them in the other side. This operation is done for both sides of the DFT output. It is noted that in the special case of $E = 0$, $Q = M$ and $X'(k) = X(k)$ for $k = 0, \ldots, Q - 1$.

The other key ingredient is to shape the transmit signal spectrum such that the effective filtered pulse-shape, denoted by $g'(.)$, yields reduced PAPR compared to the basic DFT-s-OFDM pulse-shape $g(.)$ in (4). A computationally efficient way to achieve this is by means of an element-wise multiplication between the (symmetrically extended version of the) DFT output and a frequency-domain window $W(k)$. The filtered signal can thus be formally defined as

$$X'_{\text{filtered}}(k) = X'(k)W(k), \tag{6}$$

for $k \in \{0, 1, \ldots, Q - 1\}$. Denoting the frequency-domain representation of the basic DFT-s-OFDM pulse-shape $g(n)$ by $G(k) = \mathcal{F}\{g(n)\}$, the effective filtered time-domain pulse-shape $g'(n)$ can be expressed in frequency-domain as $G'(k) = G(k)W(k)$. Thus, the effective pulse-shape can be directly controlled through the selection of $W(k)$. The design of efficient shaping responses $W(k)$ is addressed explicitly in Section II-D. We also note that the shaping can be basically applied in both cases, without and with spectral extension, while is expressed above for the general case of spectrally extended signal $X'(k)$. The zero extension situation corresponds then to the special case with $E = 0$. In terms of the involved additional computational complexity compared to the basic DFT-s-OFDM transmitter, assuming real-valued filtering weights $W(k)$, the FDSS processing requires $2(M + E)$ additional real-valued multiplications per transmitted DFT-s-OFDM symbol.

However, it is also important to note that when shaping the signal in the frequency-domain, inter sub-symbol interference (ISSI) is incurring, meaning that the different effective pulses $g'(n - \frac{mN}{M})$ and $g'(n - \frac{m'N}{M})$ are not orthogonal

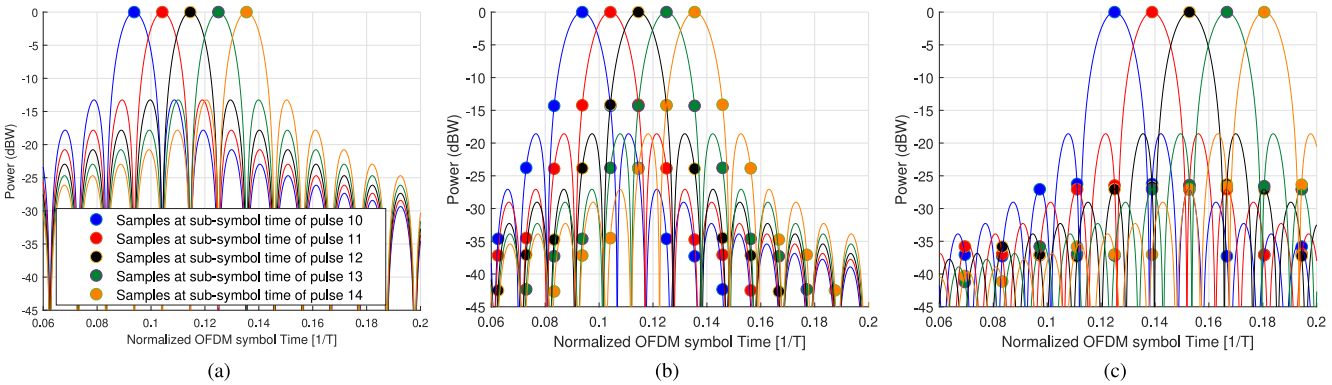


**FIGURE 2.** Effective pulses for sub-symbols number 10 to 14 within a DFT-s-OFDM symbol with $N = 1024$, for (a) traditional DFT-s-OFDM, $Q = M = 96$, (b) FDSS-based DFT-s-OFDM without spectral extension, $Q = M = 96$, and (c) FDSS-based DFT-s-OFDM with 25% spectral extension, $Q = 96$, $M = 72$.

at sub-symbol time instants for $m \neq m'$. Such appearance of ISSI degrades, in general, the quality of the received signal since the received sub-symbols are affected by the surrounding ones. However, the receiver equalizer can handle the distortion, along the actual channel effects, as long as the channel estimate utilized by the equalizer contains the combined effects of the channel and the transmitter response.

To further alleviate such unwanted degradation at the transmitter side, the utilization of non-zero excess bandwidth $E$ in the form of above-described symmetric spectral extension is beneficial, which implies transmitting $M$ complex data symbols by using $Q > M$ subcarriers. Overall, the excess bandwidth serves thus the following three functions.

- The excess band absorbs part of the ISSI, thus reducing the degradation on the error vector magnitude (EVM).
- The excess band helps on further reducing the PAPR, as the effective pulses have larger time separation.
- The excess band can also be utilized by the receiver, providing frequency diversity, thus improving the detection performance.

In order to illustrate the effect of frequency shaping and spectral extension, Fig. 2 shows the effective pulses that are modulated by the complex sub-symbols for one DFT-s-OFDM symbol duration with $Q = 96$ total allocated subcarriers. For visual simplicity, only 5 sub-symbol pulses are shown in the figure. Fig. 2(a) shows the pulses of a traditional DFT-s-OFDM modulator (i.e., the periodic sinc-like functions in (4)) with $Q = M = 96$, where at the sub-symbol time instants, only the corresponding pulse has a non-zero value. This means that no ISSI is introduced. Fig. 2(b), in turn, shows the effective pulses when a shaping filter is used but yet without spectral extension ($Q = M = 96$ subcarriers, refer to Section II-D for details on the filter design). It can be observed that ISSI is appearing since the values of the neighboring pulses are non-zero at the sub-symbol time instants. Specifically, the nearest neighboring pulses on each side contain now 14 dB less power than the central pulse at the sub-symbol time. It is also worth to note that the shaped effective pulses $g'(n)$ in Fig. 2(b) decay more rapidly than the original pulses $g(n)$ in Fig. 2(a). Finally, Fig. 2(c) shows the pulses when the same shaping filter as in Fig. 2(b) is used while now incorporating also 25% excess bandwidth ($M = 72$ and $Q = 96$ subcarriers). In effect, when excess band is utilized, the time-domain pulse-shapes are the same as in the case where no excess band was used since the shaping filter is the same, but they have now larger time-separation due to the fact that less sub-symbols are transmitted within the same DFT-s-OFDM symbol interval with the same occupied bandwidth. This larger time-separation allows to reduce the ISSI, as can also be observed in the figure where now the first neighboring pulses have 27 dB less power than the central pulse at the sub-symbol time instants.

It can also be observed in Fig. 2 that the contribution of the adjacent pulses at the vicinity of the sub-symbol instants decreases when FDSS with extension is utilized. This is because the effective pulses $g'(n)$ are more confined in time and therefore decay more rapidly than the original pulses $g(n)$. This, in turn, impacts the PAPR distribution in a favorable manner. Specifically, from (3), it is clear that the DFT-s-OFDM symbol waveform is a combination of the sequence of complex modulated sub-symbols $s(m)$, for $m \in \{0, 1, \ldots, M-1\}$, that weight the corresponding shifted pulses $g(n - \frac{mN}{M})$. Thus, when the sidelobes of the different weighted and shifted pulses add up coherently, large peaks will appear in the signal, yielding high PAPR values. However, since the pulses in the FDSS based system decay faster, lower amount of pulses contribute to the waveform between the sub-symbol instants, and as a consequence, PAPR values are lower. This will be illustrated along the numerical results in Section IV.

Finally, for presentation completeness, we note that FDSS-based DFT-s-OFDM with spectral extension can basically be interpreted as special case of GFDM [29], under specific parametrization. Specifically, the considered FDSS approach can be seen as a generalization compared to mainstream GFDM literature [30], [31], such that the involved oversampling factor is non-integer, while also allowing to operate with the natural sample rate and transform sizes of DFT-s-OFDM as standardized for 5G NR physical layer.

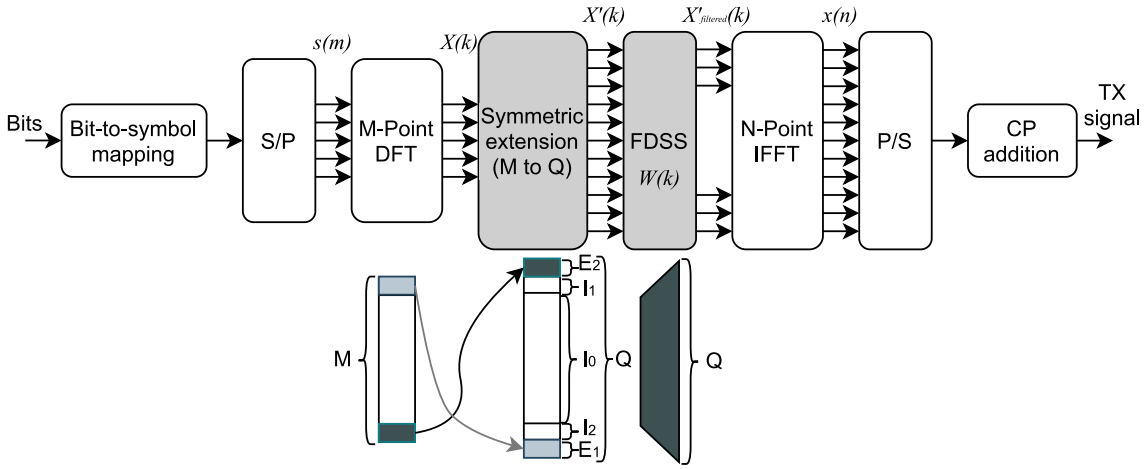


**FIGURE 3.** Block-diagram of DFT-s-OFDM transmitter with FDSS and spectral extension.

Additionally, the FDSS approach is by design free from intercarrier interference (ICI) within an individual UE signal, while in GFDM this depends again on the chosen filtering characteristics [30].

### C. FDSS AND RECEIVER ASPECTS

We next address how the adoption of the FDSS and spectral extension impact the receiving end. In general, in this work, we assume that the receiver does not have knowledge of the exact FDSS filter or shaping function used in the transmitter. This is motivated by the facts that such assumption allows for vendor-specific shaping implementations and reduces the standardization impact, while also making the FDSS processing more transparent to the receiver. To facilitate transparency, we assume that the reference signals used for channel estimation are also shaped with the same filter as the one used along data transmission. Specifically, shaping the reference signals for channel estimation serves two purposes – firstly, with the appropriate processing, it helps lowering the PAPR of the DFT-s-OFDM symbol carrying the reference signals, and secondly, the receiver does not have to be aware of the filter response utilized in transmission, which allows for implementation flexibility for the UE manufacturers. In this approach, the receiver essentially estimates the combined response of the transmitter shaping filter and the actual channel, through the received reference signals.

Then, when it comes to the excess bandwidth, the following two scenarios can basically be identified.

1) The excess bands of different UEs are not overlapping with any other transmissions, and therefore, are available for receiver processing. This type of processing can also be related to fractionally oversampling receiver processing [32].
2) The excess bands of the UEs are overlapping with other transmissions and therefore are not available for receiver processing – or the receiver is not capable of processing the excess band (basic DFT-s-OFDM receiver). This scenario also contains the case where excess bands of neighboring UEs are deliberately overlapping, thus effectively reducing the total amount of excess bandwidth in the cell or network.

We next focus on the more advanced scenario of 1), where the excess band of a particular UE is not overlapping with any other transmissions, and address further the receiver processing aspects. Specifically, a receiver capable of using and processing the excess band first estimates the joint effective channel response through the reference signals. Then, inspired by the symmetric nature of the spectral extension, the receiver can combine or sum the received samples at the excess band REs and the corresponding samples at the in-band REs. This reduces the noise enhancement in the channel equalization processing, especially at the allocation edges where the transmitter shaping filter can have larger attenuation. Finally, linear minimum mean squared error (LMMSE) frequency-domain equalization (FDE) over the in-band REs is performed, and the equalized samples are fed towards the detector.

The channel effects including the FDSS filter used in transmission and the channel between transmitter and receiver are estimated for the whole allocation bandwidth (i.e., in-band and excess band) by using the demodulation reference signals being shaped with the same FDSS filter. These reference signals are used as training sequences to estimate the effective channel [33], with the estimated channel being denoted as $\hat{H}(k)$, for $k = 0, 1, \ldots, Q-1$, in the following.

To express the receiver processing related to combining the excess band and in-band REs and the corresponding channel equalization in an explicit manner, we proceed as follows. We first denote the output of the $N$-point receiver FFT at the $Q$ allocated REs as $R(k)$, $k = 0, 1, \ldots, Q-1$. By denoting then the estimated effective channel within the total allocation bandwidth by $\hat{H}(k)$, for $k = 0, 1, \ldots, Q-1$, the received subcarrier samples are multiplied or weighted

by the conjugates of the effective channel estimates as

$$\hat{R}(k) = \hat{H}^*(k)R(k) \tag{7}$$

for $k = 0, 1, \ldots, Q-1$, where $(\cdot)^*$ denotes the complex conjugate. This essentially achieves phase equalization of the received samples, and constitutes part of the overall equalization and combining processing.

Next, similar to [34], the phased-corrected excess band subcarriers are added together with the respective in-band subcarriers. To this end, we can identify the following five frequency or spectral regions, as illustrated also in Fig. 3.

1) *Excess band 1*, $E_1$: $k \in [0, E/2-1]$. Excess band in the lower side of the spectrum allocation.
2) *In-band 2*, $I_2$: $k \in [E/2, E-1]$. In-band in the lower side of the allocation (contains copies of its REs in $E_2$).
3) *In-band 0*, $I_0$: $k \in [E, M-1]$. In-band in the middle of the allocation.
4) *In-band 1*, $I_1$: $k \in [M, E/2+M-1]$. In-band in the higher side of the allocation (contains copies of its REs in $E_1$).
5) *Excess band 2*, $E_2$: $k \in [E/2+M, Q-1]$. Excess band in the higher side of the spectrum allocation.

The cardinalities of the sets $E_1$, $E_2$, $I_1$ and $I_2$ are $|E_1| = |E_2| = |I_1| = |I_2| = E/2$, while $|I_0| = M - E$. Stemming from above, the combination of the phase-equalized excess and in-band REs can now be expressed as

$$\tilde{R}(k) = \begin{cases} \hat{R}(k) + \hat{R}(k+M) & k \in I_2 \\ \hat{R}(k) & k \in I_0 \\ \hat{R}(k) + \hat{R}(k-M) & k \in I_1 \end{cases} \tag{8}$$

Finally, to complete the LMMSE equalization for the combined in-band REs, similar combination as in (8) is carried out for the power response of the estimated channel $|\hat{H}(k)|^2$. The result of such combined power response is denoted by $|\tilde{H}(k)|^2$. Then, the in-band equalization can be completed as

$$\tilde{R}_{\text{eq}}(k) = \frac{\tilde{R}(k)}{\left|\tilde{H}(k)\right|^2 + \sigma_N^2/\sigma_X^2}, \tag{9}$$

for $k \in I_0 \cup I_1 \cup I_2$, where $\sigma_N^2$ refers to the (estimated) noise variance while $\sigma_X^2$ denotes the subcarrier domain signal power.

### D. FDSS FILTER DESIGN

In 5G NR Rel-15 and Rel-16, FDSS *without spectral extension* is basically supported for $\pi/2$-BPSK. The exact shaping function is not defined in the specifications, however, certain performance requirements are defined which yield boundary conditions for shaping filter implementations. Such approach allows UE vendors to pursue their own implementation and performance optimizations, while the system performance is guaranteed through the specified minimum requirements related to transmit signal spectral flatness, in-band/OOB emissions, and EVM [7].

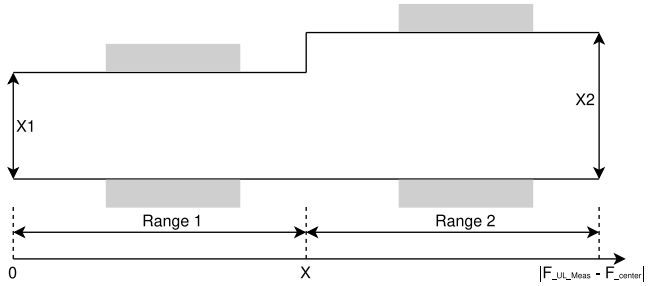


**FIGURE 4.** Principal illustration of the EVM equalizer spectral flatness requirements as defined in [7].

**TABLE 1.** Mask for EVM equalizer coefficients for $\pi/2$ BPSK with spectrum shaping, normal conditions, as defined in [7].

| Frequency range | Parameter | Maximum ripple [dB] |
|---|---|---|
| $\lvert F_{\text{UL,Meas}} - F_{\text{center}}\rvert \leq X$ [MHz] (Range 1) | $X1$ | 6 (p-p) |
| $\lvert F_{\text{UL,Meas}} - F_{\text{center}}\rvert > X$ [MHz] (Range 2) | $X2$ | 14 (p-p) |

To this end, the EVM equalizer flatness is used for defining the UE transmission spectral flatness requirements for $\pi/2$-BPSK with spectral shaping [7]. Specifically, the peak-to-peak variation of the EVM equalizer coefficients within the frequency range of the UL allocation is not allowed to exceed the specified limits. The spectral flatness requirement is defined for two frequency ranges that divide the allocation in equal-size parts [7]. This is illustrated with related parameters $X1$ and $X2$ in Fig. 4, while Table 1 shows the values, where $X$ in MHz is equal to 25% of the bandwidth of the allocation. The EVM equalizer spectral flatness requirements are, in general, inversely related to the allowed attenuation or spectral shaping within the transmit signal allocation bandwidth.

In this work, we address the shaping filter design through the so-called truncated windows or truncated filters, allowing to link the filter characteristics directly to the spectrum flatness requirements. The basic idea with truncated windows is to modify the frequency response of any known window – for example raised cosine (RC) or root raised cosine (RRC) – with the aid of two parameters: (*i*) roll-off, $\rho$, which defines the shape (or slope) of the transition band, and (*ii*) truncation factor, $\beta$, which defines the frequency shift of the transition band towards the center or edge of the allocation.

Assuming again that $Q$ denotes the total number of REs allocated to the UE, including also the excess band if such is utilized, the number of samples or bins contained within the transition band of the filter in one side of the spectrum can be expressed as

$$N_{\text{TB}} = \lfloor Q \times \rho \rfloor. \tag{10}$$

Note that the transition bandwidth is not affected by the truncation factor $\beta$. At this stage, the transition bands are placed in such a way that with $\beta = 0$, the center of the

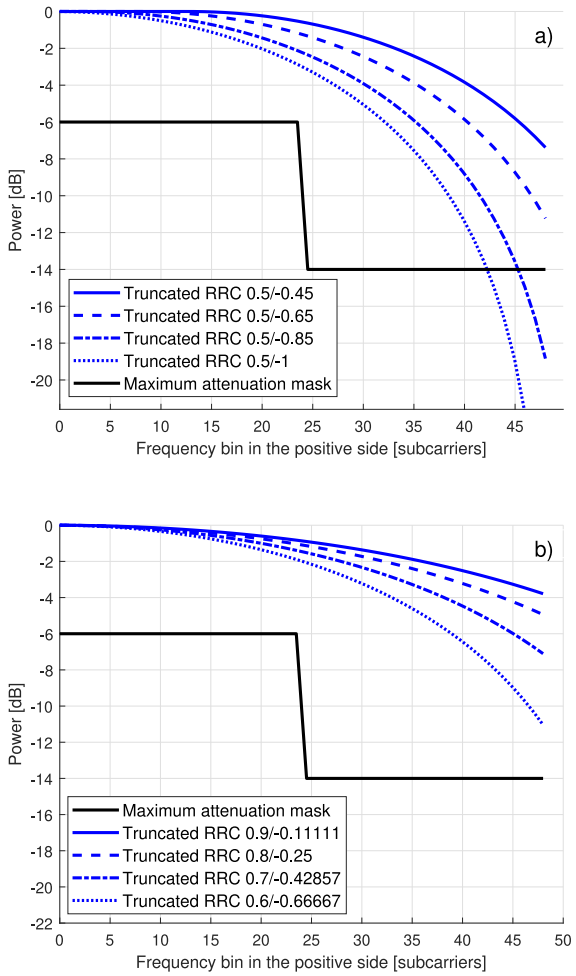


**FIGURE 5.** Examples of truncated RRC windows in the positive side of the spectrum with different roll-off and truncation factors for $Q = 96$. The legend depicts the numerical values of the roll-off ($\rho$) and truncation factor ($\beta$), expressed as $\rho/\beta$.

transition band aligns with the edge of the allocation, basically corresponding to the normal definition of RC or RRC windows in frequency-domain. The feasible values of $\beta$ are then defined as

$$\begin{aligned} -\frac{1}{2} \leq \beta \leq \frac{1}{2}, \quad &\text{if} \quad \rho \leq 0.5 \\ -\frac{(1-\rho)}{\rho} \leq \beta \leq \frac{1}{2}, \quad &\text{if} \quad \rho > 0.5. \end{aligned} \tag{11}$$

In general, the $N_{TB}$ samples of the transition band can be defined using an already known window function that can be, e.g., RC, RRC or another window function.

If the truncation factor is positive ($\beta > 0$), the frequency shift is defined to be towards the allocation edge, while for negative values of $\beta$, the shift is towards the allocation center. Now, the number or REs that the transition band is shifted can be defined as

$$N_{\text{trunc}} = \left\lfloor |\beta| \frac{N_{\text{TB}}}{2} \right\rfloor. \tag{12}$$

As a consequence of the shifting, in the passband the number of bins from the window in one side becomes

$$N_{\text{passband,TB}} = (1-\beta)\frac{N_{\text{TB}}}{2}. \tag{13}$$

Therefore, in one side, $Q/2 - N_{\text{passband,TB}}$ number of samples have to be appended whose values are equal to one.

In order to generate a shaping filter that fits inside the spectral flatness requirements, the windows can be easily tuned by means of the truncation factor. The spectral flatness requirements are directly mapped to maximum allowable attenuation in the different ranges of the spectrum. In a first attempt, the UE can generate the transition band of the filter as previously explained by selecting a given roll-off ($\rho$) and a function to generate the transition band. Once the transition band is obtained, by changing the truncation factor ($\beta$) the filter can be further tuned such that the wanted attenuation for the different ranges is obtained.

Fig. 5(a) shows examples of the positive side of the spectrum of truncated RRC filters generated with different truncation factors for a fixed roll-off, while also illustrating the maximum attenuation mask, defined by the EVM equalizer spectral flatness requirements noted previously. Additionally, Fig. 5(b) shows examples of truncated RRC filters with different roll-offs while the truncation factor is set to be the larger of the feasible negative values according to (11). It can be seen that for a fixed roll-off of $\rho = 0.5$, increasing the negative value of the truncation factor generates more attenuation at the edge of the band which can be even larger than the maximum allowed. For that reason, in the forthcoming evaluations, we have selected the truncated RRC filter with $\rho = 0.5$ and $\beta = -0.65$ since such shaping response respects the spectrum flatness requirements while avoiding excess attenuation at the edge of the band.

## III. EVALUATION METHODS AND PERFORMANCE METRICS

In the forth-coming numerical evaluations, the system performance is assessed and mutually compared covering the cases of (*i*) reference transmitter without FDSS, (*ii*) enhanced transmitter with FDSS but without extension, and (*iii*) enhanced transmitter with FDSS and spectral extension. The main transmitter related performance metrics are the transmit signal PAPR distribution and cubic metric (CM) as well as the allowed MPR subject to constraints in the passband waveform quality (EVM, and in-band emissions (IBE) limits) and out-of-band emission (occupied bandwidth (OBW), adjacent channel leakage ratio (ACLR)) as defined in [7]. This allows to assess how much larger transmit powers the FDSS based UEs are able to utilize, compared to ordinary DFT-s-OFDM transmitter, while still meeting the transmitter quality requirements. Finally, also extensive radio link performance evaluations are covered and performed, in order to obtain and assess the overall coverage gain of the proposed methods with respect to the baseline reference system without FDSS. In that context, also the differences between the normal DFT-s-OFDM receiver and the more

advanced receiver being able to process also the extension bandwidth are addressed.

In general, as noted already in Section I, PUSCH is one of the main coverage bottleneck at both FR1 and FR2 for eMBB service. Hence, we focus on PUSCH and cover both frequency ranges in the performance evaluations. The main system level reference schemes against which the proposed solutions will be compared are $\pi/2$-BPSK with FDSS without spectral extension and normal QPSK without FDSS – both of which being supported in 5G NR Rel-16 standard for the UL [7].

Next, we address and define the noted performance metrics in further details, while the actual numerical results and their analysis are then provided in Section IV.

### A. PAPR AND CUBIC METRIC

One direct metric to evaluate the transmit waveform power-efficiency is the sample-wise PAPR distribution. The so-called instantaneous PAPR is defined as the ratio between the instantaneous squared envelope and the corresponding average power of the signal, expressed as

$$PAPR(n) = \frac{|x(n)|^2}{\frac{1}{N_{\text{tot}}} \sum_{l=0}^{N_{\text{tot}}-1} |x(l)|^2}, \tag{14}$$

where $x(n)$ denotes the complex sample at time-instant $n$, and $N_{\text{tot}}$ is the overall signal length in samples. Then, the statistical behavior or distribution is commonly assessed and presented through the complementary cumulative distribution function (CCDF), while further detailed numerical comparisons are often pursued at 1%, 0.1%, or 0.01% CCDF points [35]–[37].

Additionally, CM is another commonly utilized and representative metric that is known to well characterize the PA back-off needed for the studied waveform [38]. As defined in [38], the CM can be expressed as

$$\text{CM} = \frac{\text{RCM}_{\text{dB}} - \text{RCM}_{\text{ref-dB}}}{K}, \tag{15}$$

where RCM is the raw CM in dB, defined as

$$\text{RCM}(x(n)) = 20\log\left(\sigma\left[\left(\frac{|x(n)|}{\sigma(|x(n)|)}\right)^3\right]\right), \tag{16}$$

while $\text{RCM}_{\text{ref-dB}} = 1.542$ and $K = 1.85$ are empirical factors chosen according to the system [38], and finally $\sigma(x(n))$ refers to the root mean square value of $x(n)$.

### B. MINIMUM ALLOWABLE MPR

To assess the maximum feasible output powers of the different transmit waveforms – or alternatively the minimum allowable MPRs – the signals are fed into a PA stage. The PA input power is gradually increased, while always assessing and measuring the corresponding PA output signal with respect to the all standardized UE RF requirements [7]. The power is increased until at least one standardized signal quality metric is not anymore fulfilled, yielding thus the maximum feasible output power. For realistic assessment, RF measurement based models of true UE PAs at FR1 and FR2 are used in the evaluations.

The final quantitative MPR is measured in terms of the output back-off (OBO), defined as

$$\text{OBO(dB)} = \text{P}_{\text{sat}}\text{(dBm)} - \text{P}_{\text{out}}\text{(dBm)}, \tag{17}$$

where $\text{P}_{\text{sat}}$ is the PA saturation power, and $\text{P}_{\text{out}}$ is the actual mean output power. The goal of the proposed methods is to facilitate lower OBO (larger transmit power) while still meeting the RF requirements.

The considered UE RF requirements, defined in [7], cover the following.

- *IBE:* Measure of the ratio between the power in the allocated physical resource blocks (PRBs) and the non-allocated PRBs inside the channel bandwidth.
- *EVM:* Measure of the distance between the received symbols (with a test receiver) and the original symbols.
- *OBW:* Measure of the transmit signal spectral containment, defined as the bandwidth that contains 99% of the total integrated mean power.
- *ACLR:* Another measure of the transmit signal spectral containment, particularly from the adjacent channels perspective. Defined as the ratio of filtered mean power centred at the considered channel and the corresponding mean power at the adjacent channel.

### C. LINK-LEVEL PERFORMANCE

Also the link-level performance is evaluated in terms of the coded PUSCH block error rate (BLER) covering a wide variety of different scenarios, i.e., operation at FR1 and FR2, different modulations, different allocation sizes, FDSS without and with excess band, and so forth. Also the impact of the receiver type is covered and assessed. Full coded BLER vs. SNR curves are evaluated, while then quantitative comparisons are pursued at 10% BLER level that is commonly the link adaptation operation point for first transmissions in hybrid automatic repeat request (HARQ) based networks, such as LTE and NR.

In order to obtain fair comparisons when the excess band is utilized, the code rate of the transmission is increased in the same amount as the extension to get the same spectral efficiency. For example, if 25% spectral extension is used for QPSK with FDSS, the code rate is then increased accordingly compared to that of the reference QPSK without FDSS with the same allocated PRBs.

### D. OVERALL COVERAGE GAIN

With the results obtained from the MPR/OBO analysis and the link level evaluations, the overall coverage gain (CG) is computed and quantified as

$$\text{CG} = \text{OBO}_{\text{diff}} + \text{SNR}_{\text{diff@10\%BLER}}, \tag{18}$$

where $\text{OBO}_{\text{diff}}$ is the difference in dB between the reference case and the evaluated method, and $\text{SNR}_{\text{diff@10\%BLER}}$

**TABLE 2.** Evaluation scenarios and considered parameters.

| Parameter | | Value | |
|---|---|---|---|
| | | FR1 | FR2 |
| Carrier frequency | | 3.5 GHz | 28 GHz |
| Channel BW | | 20 MHz | 400 MHz |
| Sub-carrier spacing | | 15 kHz | 120 kHz |
| Channel model [39] | | TDL-C 300 ns | TDL-A 30 ns |
| FDSS filter | | Truncated RRC ($\rho = 0.5$, $\beta = -0.65$) | |
| Spectral extension | | 0% and 25% | |
| Code rate | $\pi/2$-BPSK | QPSK | QPSK FDSS 25% ext. |
| CR0, 1/4 bps/Hz | 1/4 | 1/8 | 1/6 |
| CR1, 1/3 bps/Hz | 1/3 | 1/6 | 2/9 |
| CR2, 1/2 bps/Hz | 1/2 | 1/4 | 1/3 |
| CR3, 2/3 bps/Hz | 2/3 | 1/3 | 4/9 |
| CR4, 1 bps/Hz | N/A | 1/2 | 2/3 |

is the difference in SNR needed to achieve 10% BLER for the compared waveforms. This is assessing the true gain in the network coverage, such that differences in the needed decoder SNRs and in the feasible transmit powers are properly taken into account.

## IV. NUMERICAL RESULTS AND ANALYSIS

In this section, the obtained numerical results are presented and discussed, with the main evaluation scenarios and corresponding parameters being shown in Table 2. The shaping filter used in the evaluations corresponds to a truncated RRC with $\rho = 0.5$ and a truncation factor of $\beta = -0.65$ for all the considered modulations, i.e., $\pi/2$-BPSK and QPSK. This filter conforms to the EVM spectral flatness requirements while allows for effectively reducing the PAPR and resulting in good detection performance. Fig. 6 shows the shape of the filter for two example cases of $Q = 96$ and $Q = 3072$ subcarriers. It is important to note that the shape of the filter depends only on the allocation size ($Q$) and that it is the same for different extension factors of 0% (no extension) and 25% considered in the evaluations.

### A. PAPR AND CM DISTRIBUTIONS

The PAPR distributions for the considered modulations and FDSS/extension combinations are shown in Fig. 7. It can be clearly observed that applying FDSS without spectral extension for $\pi/2$-BPSK (supported in 5G NR Rel-15 and Rel-16) provides significant PAPR reduction performance – up to 2 dB gain at $10^{-2}$ CCDF level compared to $\pi/2$-BPSK without FDSS. However, for QPSK, applying FDSS without spectral extension provides only moderate improvements at $10^{-2}$ CCDF level, while at $10^{-1}$ CCDF level presenting actually the highest PAPR of all the considered modulations. On the other hand, when FDSS with 25% spectral extension is used for QPSK, the PAPR is reduced by 2 dB at $10^{-2}$ CCDF level, making the gain comparable to that of $\pi/2$-BPSK. These results are well-aligned with the conceptual discussion in Section II-B, such that particularly the larger time separation of the effective pulses, enabled by the spectral extension, allows for efficient PAPR reduction.

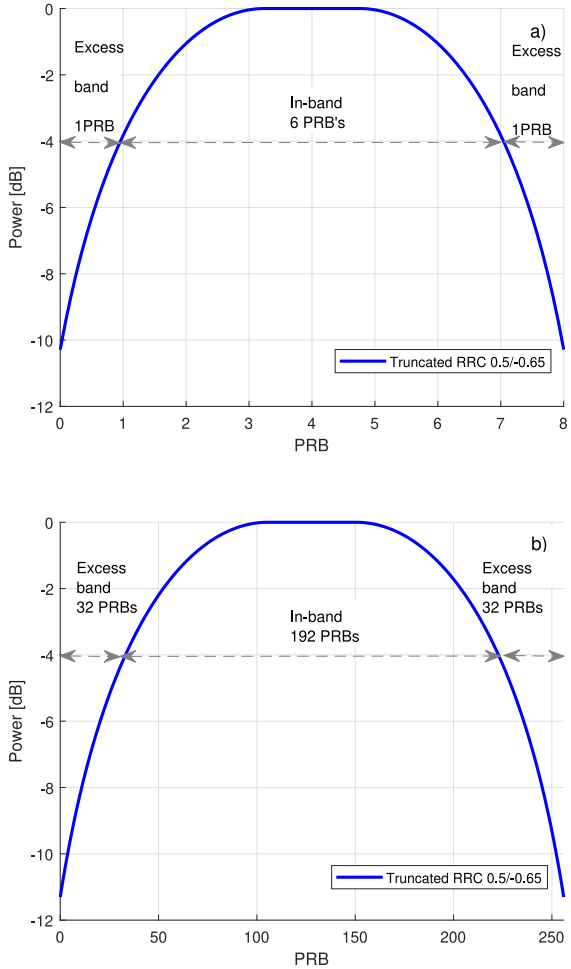


**FIGURE 6.** Truncated RRC filter with $\rho = 0.5$ and $\beta = -0.65$ used for evaluations for allocations of (a) $Q = 96$ subcarriers (8 PRBs) and (b) $Q = 3072$ subcarriers (256 PRBs). The allocation sizes at in-band and at excess band are also noted for the case of 25% extension.

Table 3 shows the corresponding CM values of the same modulation and FDSS combinations as considered in Fig. 7. For $\pi/2$-BPSK, the CM is reduced by 0.7 dB when FDSS is adopted. For QPSK, when FDSS is used without spectral extension, the CM value is essentially identical to the normal QPSK case (a minor reduction of 0.1 dB). However, when spectral extension is introduced, a very notable reduction by 0.9 dB is achieved in the CM. Thus, the conclusions are very similar to what already obtained through PAPR distributions – QPSK clearly needs or benefits from the spectral extension.

### B. OBO AT FR1 AND FR2 FOR DIFFERENT ALLOCATION SIZES

In order to obtain realistic results and measure the effects of the PAPR/CM reduction in the maximization of the PA output power, the minimum allowable OBO for the studied modulations with and without FDSS is obtained by using a 3GPP Rel-16 standard compliant emission evaluation tool. It represents the MPR and corresponds to the minimum OBO

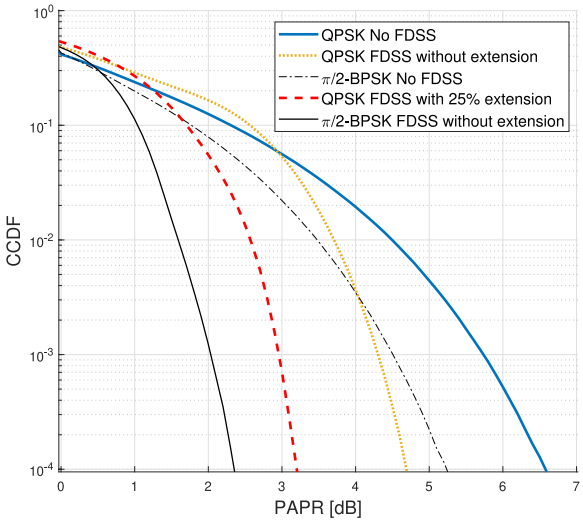


**FIGURE 7.** Instantaneous PAPR CCDFs for $\pi/2$-BPSK and QPSK with and without FDSS and spectral extension. FDSS shaping filter is the truncated RRC with $\rho = 0.5$ and $\beta = -0.65$, illustrated in Fig. 6.

**TABLE 3.** CM of $\pi/2$-BPSK and QPSK modulations with and without FDSS and spectral extension.

| Modulation/waveform | CM [dB] |
|---|---|
| QPSK No FDSS | 1.0 |
| QPSK FDSS without spectral extension | 0.9 |
| $\pi/2$-BPSK No FDSS | 0.2 |
| **QPSK FDSS with 25% spectral extension** | 0.1 |
| **$\pi/2$-BPSK FDSS without spectral extension** | -0.5 |

needed while meeting the UE RF requirements explained in Section III-B (EVM, OBW, IBE, ACLR). The PA models used in the evaluations reflect true measured terminal PA systems at FR1 and FR2.

Fig. 8 shows the obtained OBO values as functions of the allocation size ranging from 4 to 100 PRBs at FR1 and from 4 to 256 PRBs at FR2. Additionally, the limiting emission or signal quality measures are indicated in the figure. The results illustrate that substantially larger PA output powers can be obtained in the QPSK case when FDSS is combined with spectral extension. Specifically, without spectral extension, the differences in OBO between normal QPSK and QPSK with FDSS are between 0.3 and 0.8 dB at FR1, whereas when 25% extension is applied, the corresponding OBO reduction or output power gains are between 1.2 and 1.6 dB. At FR2, the mutual differences are similar. Through these results, we can clearly conclude that QPSK with FDSS while lacking spectral extension does improve the transmit power to a small extent. However, when spectral extension is also considered substantial further improvements can be obtained allowing the PA to operate clearly closer to saturation.

From the obtained OBO behavior, it can also be observed that $\pi/2$-BPSK with FDSS can still operate at lower OBO than QPSK with FDSS and spectral extension. Interestingly, however, for the PRB allocations of interest in terms of cell-edge coverage (i.e., small allocation sizes), the OBO differences are very small or even marginal. For example

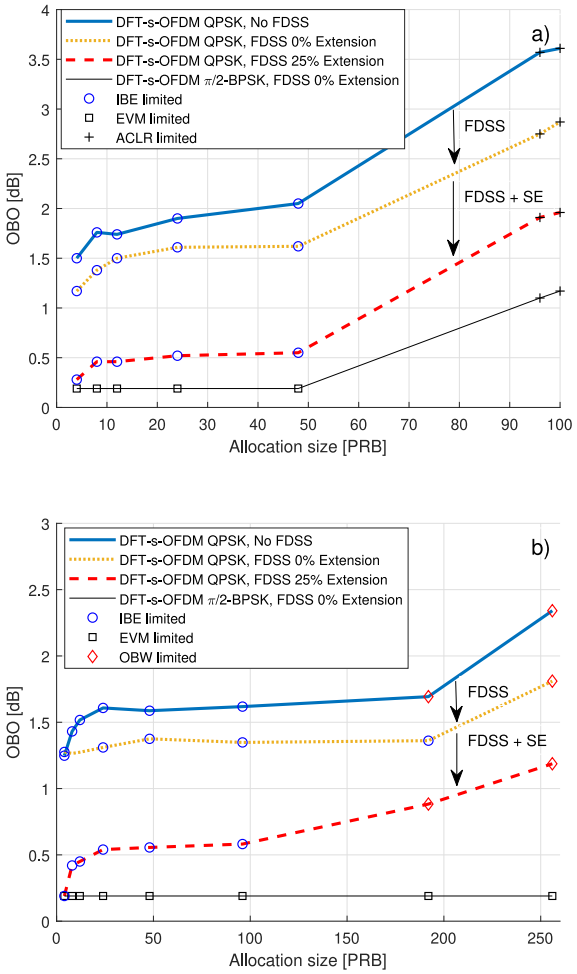


**FIGURE 8.** Obtained OBO behavior for the considered modulations with respect to PRB allocation size at (a) FR1 and (b) FR2. Also the limiting factors or measurements are high-lighted. FDSS shaping filter is the truncated RRC with $\rho = 0.5$ and $\beta = -0.65$.

with 4 PRB allocation size, the difference is smaller than 0.1 dB at FR1, and essentially 0 dB at FR2.

As for the limiting factors high-lighted also in Fig. 8, it can be observed that for all QPSK variants, IBE limits the small and medium allocations at both FR1 and FR2. For large allocations, the ACLR is the limiting factor at FR1, while at FR2 the corresponding limiting measurement is OBW. For $\pi/2$-BPSK, the main limiting factor is EVM at both FR1 and FR2, except at largest allocations at FR1, due to the fact that the PA is already very close to full saturation.

### C. RADIO LINK PERFORMANCE AT FR1 AND FR2

After understanding the MPR or OBO requirements for the different considered modulations, we next focus on the corresponding radio link performance. The evaluations focus on assessing PUSCH coded BLER performance with NR Rel-16 standard-compliant low-density parity-check (LDPC) codes. In these evaluations, two different allocation sizes are considered, namely a narrow allocation case and an almost full allocation case, which correspond to 8 and 100 PRBs at FR1, and 8 and 256 PRBs at FR2. FDSS-based QPSK

without spectral extension is not considered in these radio link evaluations due to the fact that it was observed in the previous subsection to be relatively ineffective in terms of the transmit power gain. Other essential evaluation factors such as the channel models are noted in Table 2.

Table 2 shows the five coding rate cases, CR0–CR4, considered in the full link simulations, building on the idea that the spectral efficiency for the different modulations is always maintained identical, such that the modulation comparison is fair. To this end, since QPSK with FDSS dedicates 25% of the allocation to the extension band, the coding rate is increased accordingly with respect to that of the original QPSK. Furthermore, for the indicated CR0–CR4 cases, the spectral efficiency varies from 1/4 bps/Hz up to 1 bps/Hz. Finally, the receiver schemes considered for QPSK with FDSS and spectral extension are a basic DFT-s-OFDM receiver that discards the excess bands, and the more advanced receiver that utilizes the excess band as described in Section II-C.

Fig. 9 shows the required SNR to achieve the 10% BLER at FR1 as a function of spectral efficiency (CR0–CR4) for the evaluated modulation and FDSS combinations while also addressing the impact of the receiver. It can be observed that for the lower PRB allocation size, illustrated in Fig. 9a, the performance of QPSK with FDSS and spectral extension is equivalent to that of the original QPSK for all the evaluated spectral efficiencies when the advanced receiver that is able to process the excess band is utilized. This is due to the usage of the advanced receiver, which is capable of reducing the noise enhancement in the equalization and implements the frequency combination between the excess band and the in-band, which gives frequency diversity. These two processing functions in the receiver help to compensate for the losses in the coding rate. Additionally, SNR penalties between 0.3 dB and 0.8 dB are observed when a basic receiver is considered, with increasing trend in the penalty for increasing coding rate. On the other hand, when larger allocations are considered, shown in Fig. 9b, the performance differences between the different QPSK variants are fairly similar to the narrowband case, up to spectral efficiencies of 0.5 bps/Hz. The advanced receiver is capable to compensate for the higher coding rate penalty, especially at lower spectral efficiencies, due to the excess band/in-band combination in the receiver side, that provides increase in the effective SNR. However, at larger spectral efficiencies, there is some more notable performance gap between basic QPSK and FDSS-based QPSK with spectral extension despite the advanced receiver scheme is deployed. This is because the combination processing in the advanced receiver brings more benefits for narrow allocations than for wider allocations since a given multipath channel is effectively less frequency-selective with narrow allocations compared to wider ones. Additionally, similar to the narrowband case, penalties between 0.3 dB and 0.8 dB can be observed between the basic receiver and advanced receiver cases.

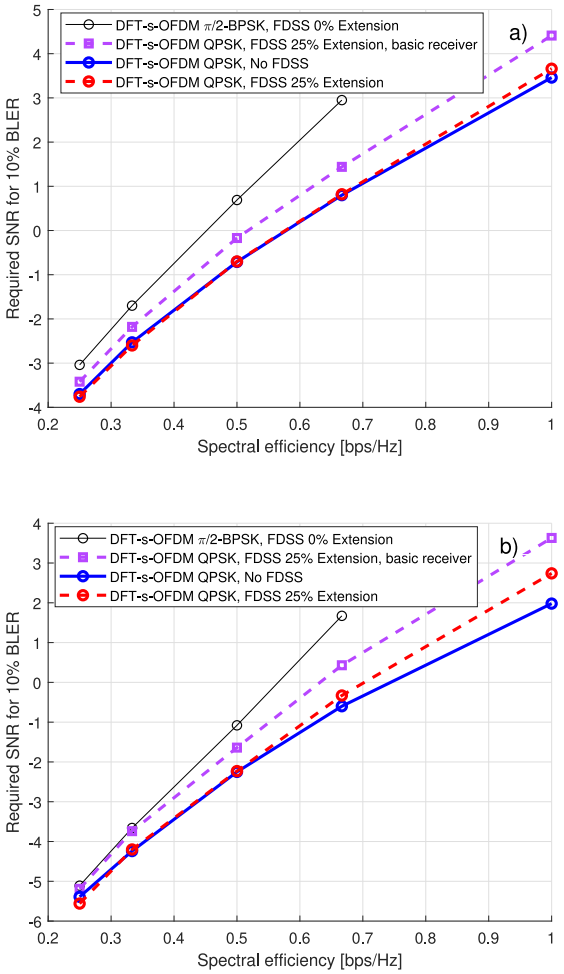


**FIGURE 9.** Required PUSCH decoding SNRs to achieve 10% BLER as functions of spectral efficiency at FR1 for (a) $Q = 96$ subcarriers (8 PRBs), and (b) $Q = 1200$ subcarriers (100 PRBs). FDSS shaping filter is the truncated RRC with $\rho = 0.5$ and $\beta = -0.65$.

Similarly, Fig. 10 shows the required SNRs to achieve the 10% BLER at FR2 for the narrowband and wideband cases with 8 and 256 allocated PRBs, respectively. In general, we can observe that FDSS-based QPSK with advanced receiver performs systematically better than at FR1, when using the corresponding normal QPSK performance as reference. In case of narrow allocation, there is even a positive performance difference of some 0.2 dB in favor of FDSS-based QPSK throughout the considered spectral efficiency range, stemming from the smaller noise enhancement of the receiver processing when spectral extension is utilized. Additionally, in case of wide allocation and higher spectral efficiencies, the penalty is smaller than in the corresponding FR1 case.

Finally, and very importantly, QPSK with FDSS and spectral extension is observed to require lower SNR than FDSS-based $\pi/2$-BPSK without extension in order to reach the same spectral efficiency in all the evaluated scenarios. Specifically, QPSK with FDSS and spectral extension is always better than $\pi/2$-BPSK, stemming partially from the

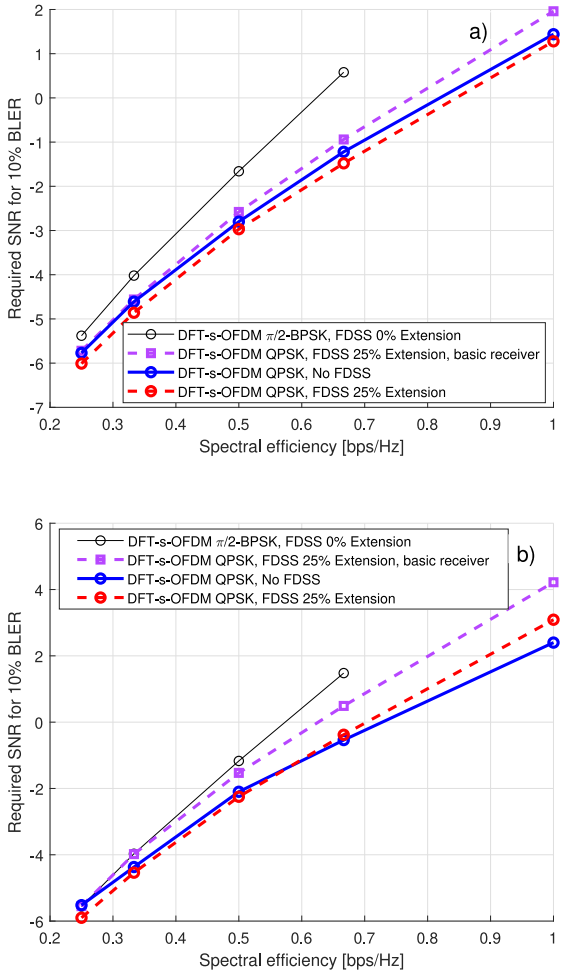


**FIGURE 10.** Required PUSCH decoding SNRs to achieve 10% BLER as functions of spectral efficiency at FR2 for (a) $Q = 96$ subcarriers (8 PRBs), and (b) $Q = 3072$ subcarriers (256 PRBs). FDSS shaping filter is the truncated RRC with $\rho = 0.5$ and $\beta = -0.65$.

ability to utilize lower coding rates, with the SNR difference ranging between 0.4 to 2 dB.

### D. OVERALL COVERAGE GAIN

Finally, by taking into account the available transmit power gains from the MPR/OBO results and the receiver decoding performance from the link-level evaluations, we are able to assess the overall coverage gain of QPSK with FDSS and spectral extension with respect to (*i*) $\pi/2$-BPSK with FDSS without spectral extension and (*ii*) normal QPSK without FDSS. To this end, by using (18) together with the previous numerical results, the overall quantitative coverage gains are obtained.

Table 4 shows the coverage gain of QPSK with FDSS and spectral extension with respect to $\pi/2$-BPSK, including both the basic and advanced receiver cases, for the narrowband and wideband allocation sizes while also covering all applicable code rates CR0–CR3. It can be observed that at FR1, with the small allocation size that is of primary interest for coverage, applying FDSS with spectral extension shows clear

**TABLE 4.** Coverage gain of QPSK with FDSS and spectral extension with respect to $\pi/2$-BPSK with FDSS without extension.

| | | | Coverage gain per code rate [dB] | | | |
|---|---|---|---|---|---|---|
| | | Alloc. size [PRB] | CR0 | CR1 | CR2 | CR3 |
| FR1 | Advanced receiver | 8 | 0.45 | 0.63 | 1.12 | 1.86 |
| | | 100 | -0.34 | -0.25 | 0.36 | 1.21 |
| | Basic receiver | 8 | 0.11 | 0.21 | 0.59 | 1.24 |
| | | 100 | -0.71 | -0.71 | -0.23 | 0.45 |
| FR2 | Advanced receiver | 8 | 0.40 | 0.61 | 1.08 | 1.83 |
| | | 256 | -0.65 | -0.42 | 0.09 | 0.87 |
| | Basic receiver | 8 | 0.11 | 0.31 | 0.69 | 1.29 |
| | | 256 | -1.00 | -0.98 | -0.63 | 0.00 |

**TABLE 5.** Coverage gain of QPSK with FDSS and spectral extension with respect to normal QPSK without FDSS.

| | | | Coverage gain per code rate [dB] | | | | |
|---|---|---|---|---|---|---|---|
| | | Alloc. size [PRB] | CR0 | CR1 | CR2 | CR3 | CR4 |
| FR1 | Advanced receiver | 8 | 1.36 | 1.37 | 1.29 | 1.28 | 1.10 |
| | | 100 | 1.82 | 1.61 | 1.63 | 1.38 | 0.89 |
| | Basic receiver | 8 | 1.02 | 0.95 | 0.76 | 0.66 | 0.35 |
| | | 100 | 1.45 | 1.15 | 1.04 | 0.62 | 0 |
| FR2 | Advanced receiver | 8 | 1.25 | 1.26 | 1.18 | 1.27 | 1.17 |
| | | 256 | 1.54 | 1.33 | 1.31 | 1.00 | 0.47 |
| | Basic receiver | 8 | 0.96 | 0.96 | 0.79 | 0.73 | 0.49 |
| | | 256 | 1.19 | 0.77 | 0.59 | 0.13 | -0.66 |

positive coverage gains for all the coding rates with respect to $\pi/2$-BPSK. The largest coverage gains are observed at highest coding rates, being 1.86 dB when the excess band is used in the receiver and 1.24 dB when the basic receiver is utilized. On the other hand, in the large allocation case, a receiver capable of using the excess band to improve the performance can provide up to 1.21 dB of coverage gain for the high coding rates. In the basic receiver case, in turn, there is smaller gain of 0.45 dB still available for CR3, while for other code rates the gain is already negative. At FR2, the tendencies are similar to those at FR1, with coverage gains available up to 1.83 dB for the small allocations and full receiver capabilities. In the large allocations, up to 0.87 dB of coverage gain can be obtained when the advanced receiver is utilized.

Similarly, Table 5 shows the coverage gain of QPSK with FDSS and spectral extension with respect to the original QPSK without FDSS. In this case, the observed coverage gains are greater than with respect to $\pi/2$-BPSK. At FR1, for the small allocation size and when using the excess band in the receiver, gains of around 1.1–1.3 dB can be obtained for all coding rates, while the corresponding gains are close to 1 dB when the basic receiver is used except for the largest coding rates. For the large allocation, gains up to 1.82 dB can be observed when deploying the advanced receiver. At FR2, the situation is fairly similar, with around 1.2 dB of gains available for the small allocations, while in case of wideband allocation, the corresponding maximum gain is

1.54 dB. These gains are reduced by 0.3–1 dB when the basic receiver is used.

### E. EFFECTS OF FDSS ON DEMODULATION REFERENCE SIGNALS

As a final technical ingredient, we address the FDSS impacts on the demodulation reference signal (DMRS) transmission. As noted already earlier, we assume that the receiver does not know the shape of the filter used in PUSCH transmission. One consequence is then that the DMRS transmitted by the UE need to be shaped with the same filter as that used for PUSCH, while covering the whole allocation (i.e., also the extension band) in the case that the advanced receiver is utilized.

In general, the 5G NR DMRS sequences are transmitted multiplexed in time with the PUSCH, which in practice means that certain DFT-s-OFDM symbols are used only for DMRS transmission, and thus the PAPR/CM distribution of the DMRS should be lower, or at least comparable to that of PUSCH. The DMRS in 5G NR Rel-15 and Rel-16 for DFT-s-OFDM can be based on low-PAPR signals where the adopted modulation is $\pi/2$-BPSK [40], or on Zadoff-Chu (ZC) sequences [25], [40] since they offer low power variations in time, generating thus signals with low PAPR/CM. It is, however, also important to note that although the Zadoff-Chu sequences have constant amplitude, they are shaped and band-limited along the transmitter processing. This causes fluctuations in the envelope and generates zero-crossings, which impact the actual PAPR of the waveform.

A Zadoff-Chu sequence of length $N_{ZC}$ can, in general, be obtained as

$$z_i^u = e^{j\frac{\pi ui(i+1)}{N_{ZC}}}, \tag{19}$$

where $u$ is the root index. The number of root indices that generate different ZC sequences is the number of integers that are relative prime to $N_{ZC}$. Hence, ZC sequences with a prime length are important since they allow the maximum amount of different ZC sequences. The DMRS generation utilizes extended ZC sequences, based on the longest prime-length ZC sequence of length $N_{ZC}$ that is smaller or equal to the desired length $M_{ZC}$. The sequence is then cyclically extended up to the desired sequence length.

However, if the DMRS generation is treated in the same way as PUSCH processing – i.e., $M_{ZC}$ bins symmetrically extended to $Q$ following by filtering/shaping – a significant increase of PAPR and CM occurs. For that reason, we propose to perform a modified spectral extension with the DMRS sequences that uses the cyclic extension defined in 5G NR Rel-16 [40] to be applied in both sides of the extension while maintaining the samples in the in-band unmodified. This approach is shown through numerical results to result in a substantially lower PAPR and CM after the frequency-domain filtering, compared to symmetric extension and FDSS. Assuming that the DMRS sequence can be derived from the same ZC sequence as in 5G NR Rel-15 and Rel-16, the proposed extension can be then described as follows.

**TABLE 6.** Example of RE mapping of ZC sequence using symmetric extension. $Q = 96$, $M = 72$, $\alpha = 4/3$, $N_{ZC} = 31$, $M_{ZC} = 36$.

| RE index | PRB index | | | | | | | |
|---|---|---|---|---|---|---|---|---|
| | 0 | 1 | 2 | 3 | 4 | 5 | 6 | 7 |
| 0 | $z_{30}$ | $z_0$ | $z_6$ | $z_{12}$ | $z_{18}$ | $z_{24}$ | $z_{30}$ | $z_0$ |
| 2 | $z_0$ | $z_1$ | $z_7$ | $z_{13}$ | $z_{19}$ | $z_{25}$ | $z_0$ | $z_1$ |
| 4 | $z_1$ | $z_2$ | $z_8$ | $z_{14}$ | $z_{20}$ | $z_{26}$ | $z_1$ | $z_2$ |
| 6 | $z_2$ | $z_3$ | $z_9$ | $z_{15}$ | $z_{21}$ | $z_{27}$ | $z_2$ | $z_3$ |
| 8 | $z_3$ | $z_4$ | $z_{10}$ | $z_{16}$ | $z_{22}$ | $z_{28}$ | $z_3$ | $z_4$ |
| 10 | $z_4$ | $z_5$ | $z_{11}$ | $z_{17}$ | $z_{23}$ | $z_{29}$ | $z_4$ | $z_5$ |

**TABLE 7.** Example of RE mapping of ZC sequence using modified extension. $Q = 96$, $M = 72$, $\alpha = 4/3$, $N_{ZC} = 31$, $M_{ZC} = 36$.

| RE index | PRB index | | | | | | | |
|---|---|---|---|---|---|---|---|---|
| | 0 | 1 | 2 | 3 | 4 | 5 | 6 | 7 |
| 0 | $z_{25}$ | $z_0$ | $z_6$ | $z_{12}$ | $z_{18}$ | $z_{24}$ | $z_{30}$ | $z_5$ |
| 2 | $z_{26}$ | $z_1$ | $z_7$ | $z_{13}$ | $z_{19}$ | $z_{25}$ | $z_0$ | $z_6$ |
| 4 | $z_{27}$ | $z_2$ | $z_8$ | $z_{14}$ | $z_{20}$ | $z_{26}$ | $z_1$ | $z_7$ |
| 6 | $z_{28}$ | $z_3$ | $z_9$ | $z_{15}$ | $z_{21}$ | $z_{27}$ | $z_2$ | $z_8$ |
| 8 | $z_{29}$ | $z_4$ | $z_{10}$ | $z_{16}$ | $z_{22}$ | $z_{28}$ | $z_3$ | $z_9$ |
| 10 | $z_{30}$ | $z_5$ | $z_{11}$ | $z_{17}$ | $z_{23}$ | $z_{29}$ | $z_4$ | $z_{10}$ |

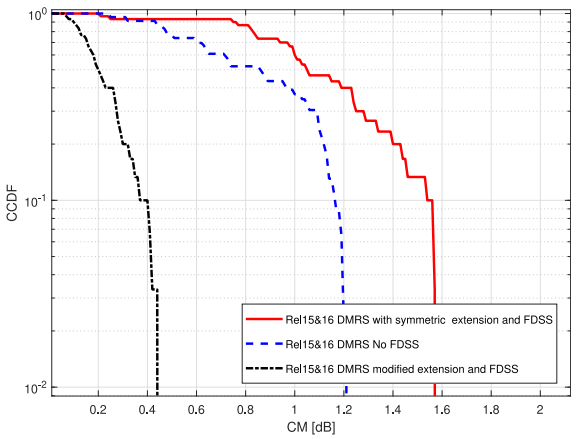


**FIGURE 11.** Cubic metric distributions of 5G NR Rel-15 and Rel-16 DMRS sequences with symmetric extension and with modified extension when applying FDSS. Also the CM distribution of the original DMRS sequences without FDSS is shown for reference. $Q = 96$ subcarriers, $M = 72$ subcarriers, $\alpha = 4/3$, $N_{ZC} = 31$, $M_{ZC} = 36$.

1) Perform cyclic shift in frequency by $\frac{1}{2}(M_{ZC} - N_{ZC} + 1)$ resource elements;
2) Adopt symmetric extension in frequency to length $\alpha M_{ZC} + 1$;
3) Truncate to desired length $\alpha M_{ZC}$;

In above, $\alpha$ denotes the extension factor that can be expressed as

$$\alpha = \frac{Q}{M}. \tag{20}$$

The DMRS sequences are mapped to every other RE inside of the allocation, which means that $\alpha M_{ZC} = \frac{Q}{2}$. Table 6 shows the resulting mapping using symmetric extension while Table 7 shows an example of the resource element mapping of extended DMRS sequence using the proposed

modified extension. Fig. 11 illustrates then the difference in the CM values for 5G NR Rel-15 and Rel-16 DMRS sequences when either directly applying symmetric extension and FDSS or when applying the modified extension approach, with the same base sequences. One CM value is obtained for each of the different Zadoff-Chu sequences that can be generated by the different root indexes, while the distribution of all these is then depicted in Fig. 11. As can be observed, there are remarkable differences in the CM distributions among the three considered cases. Additionally, it can be noted that the modified extension provides support for transparent implementation of FDSS with spectrum extension because the in-band REs contain the cyclically extended ZC sequences used in 5G NR Rel-15 and Rel-16, i.e., in the in-band, the mapped ZC coefficients are the same as in 5G NR Rel-15 and Rel 16. Hence, basic receivers can perform the channel estimation similar to existing Rel-15 and Rel-16 networks.

## V. CONCLUSION

In this article, computationally efficient solutions for UL coverage enhancement in 5G NR networks were described. Specifically, the concept of frequency-domain spectral shaping (FDSS) combined with spectral extension was introduced, with specific emphasis on improving the QPSK power-efficiency in DFT-s-OFDM based UL transmission. To this end, the basic transmitter signal processing and the associated frequency-domain shaping window design were described and addressed. Furthermore, an efficient receiver structure capable of processing the extension bandwidth and thereon to reducing the noise enhancement in the equalization phase was also devised. An extensive set of numerical performance results was provided, comparing normal QPSK, FDSS-based QPSK without spectral extension, FDSS-based QPSK with spectral extension, and FDSS-based $\pi/2$-BPSK without spectral extension, in terms of transmit waveform PAPR distributions and cubic metrics, achievable transmit powers under realistic nonlinear PA models while still fulfilling transmit signal quality requirements, achievable radio link performance, and finally the overall corresponding coverage gains in FR1 and FR2 networks.

The obtained results show that FDSS-based QPSK, especially when spectral extension is deployed, can facilitate substantially larger transmit powers compared to normal QPSK. Specifically, the observed transmit power gains were between 1–1.7 dB, which represent very notable gains. Additionally, with narrow allocations that are of primary interest for cell-edge coverage, it was shown that FDSS-based QPSK with spectral extension can support essentially the same transmit power as FDSS-based $\pi/2$-BPSK, while still offering substantially better spectral efficiency. Through the radio link coded BLER results, it was shown that FDSS-based QPSK with spectral extension can reach the normal QPSK link performance, especially when the advanced receiver capable of combining the excess band along the equalization stage is adopted. Additionally, for larger spectral efficiencies, QPSK variants were shown to outperform FDSS-based $\pi/2$-BPSK in radio link performance. Finally, when combining the transmit power results and radio link results, the true coverage gains were assessed. The results show the FDSS-based QPSK with spectral extension can provide systematic coverage gains against both normal QPSK and FDSS-based $\pi/2$-BPSK, ranging typically between 0.4–1.8 dB, especially when the advanced receiver is utilized and narrow allocations are considered. Finally, the impact of FDSS on UL DMRS transmission was addressed, and a specific modified spectrum extension approach was devised such that spectrum shaping helps also improving the coverage of the reference signals.

For future research, extension of the considered scheme for larger modulation orders is one important topic. Additionally, developing time-frequency and spatio-temporal waveform shaping methods that provide increased robustness against the effects of other analog/RF non-idealities, such as low-resolution digital-to-analog and analog-to-digital converters as well as RF oscillator phase noise, is a very important research area. Finally, the modulation and waveform solutions for 6G physical-layer are still completely open, forming thus an exciting and timely topic for future radio research.

## REFERENCES


[1] M. Giordani, M. Polese, M. Mezzavilla, S. Rangan, and M. Zorzi, "Toward 6G networks: Use cases and technologies," *IEEE Commun. Mag.*, vol. 58, no. 3, pp. 55–61, Mar. 2020.

[2] S. Rangan, T. S. Rappaport, and E. Erkip, "Millimeter-wave cellular wireless networks: Potentials and challenges," *Proc. IEEE*, vol. 102, no. 3, pp. 366–385, Mar. 2014.

[3] P. M. Asbeck, N. Rostomyan, M. Özen, B. Rabet, and J. A. Jayamon, "Power amplifiers for mm-wave 5G applications: Technology comparisons and CMOS-SOI demonstration circuits," *IEEE Trans. Microw. Theory Techn.*, vol. 67, no. 7, pp. 3099–3109, Jul. 2019.

[4] *Revised SID on Study on NR Coverage Enhancements*, document RAN Meeting #88, RP-200861, 3GPP, Gothenburg, Sweden, Jun. 2020.

[5] A. Rico-Alvarino *et al.*, "An overview of 3GPP enhancements on machine to machine communications," *IEEE Commun. Mag.*, vol. 54, no. 6, pp. 14–21, Jun. 2016.

[6] *New SID on NR Coverage Enhancement*, document TSG RAN Meeting #86, RP-193240, 3GPP, Gothenburg, Sweden, Dec. 2019.

[7] *User Equipment (UE) Radio Transmission and Reception; Part 2: Range 2 Standalone, Technical Specification Group Radio Access Network Rel-16*, 3GPP Standard TS 38.101-2 V16.2.0, Dec. 2019.

[8] "Requirements, evaluation criteria and submission templates for the development of IMT-2020, RP-182030," Int. Telecommun. Union, Geneva, Switzerland, ITU-Recommendation M.2411-0, Nov. 2017.

[9] "3rd generation partnership project; technical specification group radio access network;study on NR coverage enhancements release 17," 3GPP, Sophia Antipolis, France, 3GPP Rep. TR 38.830, Aug. 2020.

[10] S. Moloudi *et al.*, "Coverage evaluation for 5G reduced capability new radio (NR-RedCap)," *IEEE Access*, vol. 9, pp. 45055–45067, 2021.

[11] P. Annamalai, J. Bapat, and D. Das, "Constellation constraining-based coverage enhancement technique for MTC devices in LTE-A," *IEEE Wireless Commun. Lett.*, vol. 5, no. 6, pp. 596–599, Dec. 2016.

[12] S. Ravi, P. Zand, M. El Soussi, and M. Nabi, "Evaluation, modeling and optimization of coverage enhancement methods of NB-IoT," in *Proc. IEEE 30th Annu. Int. Symp. Pers. Indoor Mobile Radio Commun. (PIMRC)*, Istanbul, Turkey, Sep. 2019, pp. 1–7.

[13] *Discussion on Approaches and Solutions for NR PUSCH Coverage Enhancement*, document 3GPP TSG RAN WG1 #103, Nokia R1-2008703, 3GPP, Gothenburg, Sweden, Nov. 2020.

[14] I. P. Nasarre, T. Levanen, and M. Valkama, "Constrained PSK: Energy-efficient modulation for sub-THz systems," in *Proc. IEEE Int. Conf. Commun. Workshops (ICC Workshops)*, Dublin, Ireland, Jun. 2020, pp. 1–7.
[15] Y. Levinbook, D. Ezri, and E. Melzer, "Low-PAPR OFDM-based waveform for fifth-generation cellular communications," in *Proc. IEEE Int. Conf. Microw. Antennas Commun. Electron. Syst. (COMCAS)*, Tel-Aviv, Israel, Nov. 2017, pp. 1–6.
[16] Y. Hu, F. Wang, and J. Lu, "Low PAPR filter bank single carrier for 5G mMTC," *IEEE Internet Things J.*, vol. 6, no. 4, pp. 6887–6895, Aug. 2019.
[17] J. Armstrong, "Peak-to-average power reduction for OFDM by repeated clipping and frequency domain filtering," *Electron. Lett.*, vol. 38, no. 5, pp. 246–247, Feb. 2002.
[18] J. Hou, J. Ge, and F. Gong, "Tone reservation technique based on peak-windowing residual noise for PAPR reduction in OFDM systems," *IEEE Trans. Veh. Technol.*, vol. 64, no. 11, pp. 5373–5378, Nov. 2015.
[19] S. Gronemeyer and A. McBride, "MSK and offset QPSK modulation," *IEEE Trans. Commun.*, vol. 24, no. 8, pp. 809–820, Aug. 1976.
[20] X. Zhang, L. Chen, J. Qiu, and J. Abdoli, "On the waveform for 5G," *IEEE Commun. Mag.*, vol. 54, no. 11, pp. 74–80, Nov. 2016.
[21] G. Fettweis, M. Krondorf, and S. Bittner, "GFDM—Generalized frequency division multiplexing," in *Proc. IEEE 69th Veh. Technol. Conf. (VTC Spring)*, Barcelona, Spain, 2009, pp. 1–4.
[22] J. Nunes, P. Bento, M. Gomes, R. Dinis, and V. Silva, "Block-windowed burst OFDM: A high-efficiency multicarrier technique," *Electron. Lett.*, vol. 50, no. 23, pp. 1757–1759, 2014.
[23] T. Fernandes, M. Gomes, V. Silva, and R. Dinis, "Time-interleaved block-windowed burst OFDM," in *Proc. IEEE 84th Veh. Technol. Conf. (VTC-Fall)*, Montreal, QC, Canada, 2016, pp. 1–5.
[24] E. Dahlman, S. Parkvall, and J. Sköld, *4G: LTE/LTE-Advanced for Mobile Broadband*, 1st ed. New York, NY, USA: Academic, 2013.
[25] E. Dahlman, S. Parkvall, and S. Johan, *5G NR: The Next Generation Wireless Access Technology*, 1st ed. London, U.K.: Academic, 2018.
[26] F. A. El-samie, F. S. Al-Kamali, and A. Y. Al-nahari, *SC-FDMA for Mobile Communications*. Boca Raton, FL, USA: CRC Press, Oct. 2017.
[27] J. Ji, G. Ren, and H. Zhang, "PAPR reduction in coded SC-FDMA systems via introducing few bit errors," *IEEE Commun. Lett.*, vol. 18, no. 7, pp. 1258–1261, Jul. 2014.
[28] *DFT-Spread OFDM With Pulse Shaping Filter in Frequency Domain in Evolved UTRA Uplink*, document 3GPP TSG RAN WG1 #42, NTT DoCoMo, NEC, SHARP R1-050702, 3GPP, Gothenburg, Sweden, Sep. 2005.
[29] A. Sahin, R. Yang, E. Bala, M. C. Beluri, and R. L. Olesen, "Flexible DFT-S-OFDM: Solutions and challenges," *IEEE Commun. Mag.*, vol. 54, no. 11, pp. 106–112, Nov. 2016.
[30] N. Michailow and G. Fettweis, "Low peak-to-average power ratio for next generation cellular systems with generalized frequency division multiplexing," in *Proc. Int. Symp. Intell. Signal Process. Commun. Syst.*, Naha, Japan, 2013, pp. 651–655.
[31] N. Michailow, I. Gaspar, S. Krone, M. Lentmaier, and G. Fettweis, "Generalized frequency division multiplexing: Analysis of an alternative multi-carrier technique for next generation cellular systems," in *Proc. Int. Symp. Wireless Commun. Syst. (ISWCS)*, Paris, France, 2012, pp. 171–175.
[32] R. D. Gitlin and S. B. Weinstein, "Fractionally-spaced equalization: An improved digital transversal equalizer," *Bell Syst. Techn. J.*, vol. 60, no. 2, pp. 275–296, Feb. 1981.
[33] S. M. Kay, *Fundamentals of Statistical Signal Processing: Estimation Theory*. Englewood Cliffs, NJ, USA: Prentice-Hall, 1993.
[34] Y. Yang, T. Ihalainen, M. Rinne, and M. Renfors, "Frequency-domain equalization in single-carrier transmission: Filter bank approach," *EURASIP J. Adv. Signal Process.*, vol. 2007, 2007, Art. no. 010438. [Online]. Available: https://doi.org/10.1155/2007/10438
[35] F.-L. Luo, Ed., *Digital Front-End in Wireless Communications and Broadcasting*. Cambridge, U.K.: Cambridge Univ. Press, 2011.
[36] Y.-C. Wang and Z.-Q. Luo, "Optimized iterative clipping and filtering for PAPR reduction of OFDM signals," *IEEE Trans. Commun.*, vol. 59, no. 1, pp. 33–37, Jan. 2011.
[37] X. Zhu, W. Pan, H. Li, and Y. Tang, "Simplified approach to optimized iterative clipping and filtering for PAPR reduction of OFDM signals," *IEEE Trans. Commun.*, vol. 61, no. 5, pp. 1891–1901, May 2013.
[38] *Comparison of PAR and Cubic Metric for Power De-rating*, document 3GPP TSG RAN WG1 #37, Motorola R1-040642, 3GPP, Gothenburg, Sweden, May 2004.
[39] "Study on channel model for frequencies from 0.5 to 100 GHz; technical specification group radio access network," 3GPP, Sophia Antipolis, France, 3GPP Rep. TR 38.901 V15.1.0, Sep. 2019.
[40] "3rd generation partnership project; technical specification group radio access network; 5G; NR;physical channels and modulation," 3GPP, Sophia Antipolis, France, 3GPP Rep. TR 38.211 V16.3.0 Release 16, Nov. 2020.

**ISMAEL PERUGA NASARRE** received the B.Sc. and M.Sc. degrees from the University of Zaragoza, Spain, in 2017 and 2019, respectively. He is currently with the Department of Electrical Engineering, Tampere University, Finland. His current research interests include physical layer design for mobile communications, 5G evolution for coverage enhancements, and mmWave and sub-THz communications.

**TONI LEVANEN** received the M.Sc. and D.Sc. degrees from the Tampere University of Technology, Finland, in 2007 and 2014, respectively. He is currently with Nokia Mobile Networks, Finland. In addition to his contributions in academic research, he has worked in industry on wide variety of development and research projects. His current research interests include physical layer design for 5G NR, interference modeling in 5G cells, and high-mobility support in millimeter-wave communications.

**KARI PAJUKOSKI** received the B.S.E.E. degree from the Oulu University of Applied Sciences in 1992. He is a Fellow of the Nokia Bell Labs. He has a broad experience from cellular standardization, link and system simulation, and algorithm development for products. He has more than 100 issued U.S. patents, from which more than 50 have been declared "standards essential patents." He has authored or coauthored more than 300 standards contributions and 30 publications, including conference proceedings, journal contributions, and book chapters.

**ARTO LEHTI** received the M.Sc. degree from the University of Oulu in 2001. He is a Senior Research Specialist with Nokia standardization research. He has experience of cellular standardization both as delegate (3GPP RAN WG1, WG4, and RAN) and as a Backoffice Researcher. He has also worked on algorithm design and link/system simulations.

**ESA TIIROLA** received the M.S.E.E. degree from the University of Oulu in 1998. He is currently with Nokia Standards, where he is working on various topics related to radio research and standardization. He has more than 130 issued U.S. patents. His current research interests include signal processing and physical layer design for 5G evolution.

**MIKKO VALKAMA** (Senior Member, IEEE) received the D.Sc. (Tech.) degree (with Hons.) from the Tampere University of Technology, Finland, in 2001. In 2003, he was with the Communications Systems and Signal Processing Institute, SDSU, San Diego, CA, USA, as a Visiting Research Fellow. He is currently a Full Professor and the Department Head of Electrical Engineering, at the newly formed Tampere University, Finland. His general research interests include radio communications, radio localization, and radio-based sensing, with particular emphasis on 5G and 6G mobile radio networks.